Biological Psychiatry

Techniques and Methods

Immersion Fixation and Staining of Multicubic Millimeter Volumes for Electron Microscopy–Based Connectomics of Human Brain Biopsies

Neha Karlupia, Richard L. Schalek, Yuelong Wu, Yaron Meirovitch, Donglai Wei, Alexander W. Charney, Brian H. Kopell, and Jeff W. Lichtman

ABSTRACT

Connectomics allows mapping of cells and their circuits at the nanometer scale in volumes of approximately 1 mm^3. Given that the human cerebral cortex can be 3 mm in thickness, larger volumes are required. Larger-volume circuit reconstructions of human brain are limited by 1) the availability of fresh biopsies; 2) the need for excellent preservation of ultrastructure, including extracellular space; and 3) the requirement of uniform staining throughout the sample, among other technical challenges. Cerebral cortical samples from neurosurgical patients are available owing to lead placement for deep brain stimulation. Described here is an immersion fixation, heavy metal staining, and tissue processing method that consistently provides excellent ultrastructure throughout human and rodent surgical brain samples of volumes $2 \times 2 \times 2$ mm^3 and up to 37 mm^3 with one dimension $\leq$2 mm. This method should allow synapse-level circuit analysis in samples from patients with psychiatric and neurologic disorders.

https://doi.org/10.1016/j.biopsych.2023.01.025

The human brain is a vastly complicated tissue, and little is known about its microstructure, particularly the synaptic connectivity of its highly diverse and numerous neuronal cell types (1). These synaptic connections underlie our cognitive capabilities, and it is likely that their disruption gives rise to many presently incurable brain disorders. Recent advances in mapping nerve cell connectivity have come from connectomics via serial-section electron microscopy (EM), which provides neuronal connectivity data at synaptic resolution (2–13). To study normal, and potentially disordered, human brain microstructure, cortical samples can be collected from patients with neurologic and psychiatric disorders undergoing neurosurgical interventions (14–17).

Although most nonhuman studies preserve tissue with transcardiac perfusion (2,4,5,11,18–20), immersion fixation is the only option for human biopsies generated in the clinical setting (21–27). Furthermore, in most immersion studies, the tissue volumes are much smaller than what would be required for full-thickness cortical neural circuits in humans ($\geq 3 \times 1 \times 1$ mm^3). In addition to excellent fixation, heavy metal staining needs to uniformly penetrate large surgical biopsies for EM. This article describes a protocol for immersion fixation, heavy metal staining, and tissue processing that consistently provides excellent ultrastructure and maintenance of extracellular space (ECS) for full-thickness cerebral cortex biopsies ($\geq$8 mm^3).

METHODS AND MATERIALS

Human brain biopsies were collected in collaboration with the Icahn School of Medicine at Mount Sinai, as approved by the institutional review boards at both Mount Sinai and Harvard University. Fourteen biopsies were collected from the sites of lead placement in the prefrontal cortex for deep brain stimulation. All brain biopsy samples were collected from patients who had provided informed consent for sample collection and public sharing of deidentified data. We also collected brain samples from adult C57BL/6 mice. All animal procedures were performed according to National Institutes of Health guidelines and approved by the Institutional Animal Care and Use Committee at Harvard University.

To obtain the human samples, the neurosurgeon drilled a burr hole in the frontal bone and made a pial incision to obtain a multicubic millimeter cortical biopsy using a bio punch via microdissection (L.E. Liharska, M.S., *et al*., unpublished data, 2023). The biopsy was placed on a dampened gauze pad and was removed from the sterile field. Using a metal probe to guide it, the biopsy was transferred into a vial containing 2 mL of cold fixative (Table 1) and sealed. The time from biopsy extraction to immersion fixation was $\leq$60 seconds. The biopsy was later transferred to a larger volume of chilled fixative and stored at 4 °C until staining. Large biopsies were cut to smaller blocks $\leq 4 \times 4 \times 4$ mm^3 during the first 24 hours after extraction (Table 1 and Figure 1A).

SEE COMMENTARY ON PAGE 285

 ISSN: 0006-3223

Table 1. Method for Collection, Immersion Fixation, and Heavy Metal Staining of 2 × 2 × 2 mm^3 Brain Tissue Blocks

Step	Process	Time	Temperature	Notes
Collection and Immersion Fixation of Human and Mouse Biopsies				
Step 1a	Human: Rapidly transfer the excised neurosurgical biopsy to a small vial containing 2–4 mL of cold fixative (see *)	1–5 min	4 °C	Critical: Prepare fresh fixative within 1–2 h of use and keep it at 4 °C
	Transfer biopsy to larger volume (50–100 mL) of cold fixative	Within 5 min of excision		
	Cut biopsies into volumes no larger than 4 × 4 × 4 mm^3 and return to cold fixative	≤24 h after excision		
	Store in refrigerator for days to weeks, depending on biopsy volume	3–28 days		
Step 1b	Mouse: Anesthetize an adult mouse with isoflurane, euthanize by cervical dislocation, and remove the brain	1–2 min	RT	
	Place the brain in petri dish containing cold fixative on ice and punch or excise 2 × 2 × 2 mm^3 tissue blocks	1–3 min	4 °C	
	Transfer these blocks to 20-mL vials containing cold fixative and store in refrigerator	72 h		
	*Fixative: 2.5% GA, 2% PFA, 2mM $CaCl_2$ in 0.15M NaC buffer with 3% mannitol (445 mOsm), pH 7.4			
Heavy Metal Processing of 2 × 2 × 2 mm^3 Blocks or Blocks With Smallest Dimension = 2 mm				
Step 2	Buffer wash: 0.15M NaC (pH 7.4) + 2mM $CaCl_2$	1 × 30 min	4 °C	
		2 × 30 min	RT	
Step 3	2% OsO_4 in 0.15M NaC (pH 7.4) + 2mM $CaCl_2$	3 h	RT	
	Replace with fresh 2% OsO_4 in 0.15M NaC (pH 7.4) + 2mM $CaCl_2$	8–12 h	4 °C	
Step 4	Buffer wash: 0.15M NaC (pH 7.4) + 2mM $CaCl_2$	3 × 15 min	RT	
Step 5	2.5% potassium ferrocyanide, in 0.15M NaC (pH 7.4) + 2mM $CaCl_2$	3.3 h	RT	
Step 6	Buffer wash: 0.15M NaC (pH 7.4) + 2mM $CaCl_2$	3 × 30 min	RT	
Step 7	Filtered, 0.8% (W/V) TCH in normal saline + 1.2% mannitol	45 min	RT	
Step 8	Distilled water wash following double rinse with NS	1 × 40 min	RT	
		2 × 30 min	RT	
Step 9	2% aqueous OsO_4	5 h	4 °C	
Step 10	Distilled water wash	3 × 30 min	4 °C	
Step 11	2% aqueous uranyl acetate	8–12 h	4 °C	
		2 h	RT	
Step 12	Distilled water wash	3 × 45 min	RT	
Step 13	Dehydration with graded acetonitrile in distilled water		RT	
	10% acetonitrile/90% distilled water	20 min		
	25% acetonitrile/75% distilled water	20 min		
	50% acetonitrile/50% distilled water	20 min		
	75% acetonitrile/25% distilled water	15 min		
	100% acetonitrile	2 × 15 min		
Step 14	Infiltration with series dilution of resin (see #) in acetonitrile		RT	Critical: Prepare fresh resin for 75% and 100% resin exchange
	25% resin/75% acetonitrile	4 h		
	50% resin/50% acetonitrile	12 h		
	75% resin/25% acetonitrile	12–18 h		
	100% resin (includes 1 exchange with fresh resin)	24 h		
	#Resin: LX-112 (31.28 g), NMA (19.4 g), NSA (9.4 g), and BDMA (1.2 g)			
Step 15	Embedding in 100% LX-112 resin (recipe in step 14)	–	RT	
Step 16	Curing	4 h	45 °C	
		68 h	60 °C	

Description of steps for collection, immersion fixation, and heavy metal processing of human and mouse brain biopsy samples of volume 2 × 2 × 2 (8) mm^3 and of volume >8 mm^3 with at least one dimension ≤2 mm. All solutions (steps 2–15) are prepared fresh. Incubation at each step is done in 15- to 20-mL solutions. See the Key Resources Table for reagent details.

BDMA, N,N-dimethyl benzylamine; GA, glutaraldehyde; NaC, sodium cacodylate; NMA, methyl 5-norbornene-2,3-dicarboxylic anhydride; NSA, nonenyl succinic anhydride modified; NS, normal saline; PFA, paraformaldehyde; RT, room temperature; TCH, thiocarbohydrazide.

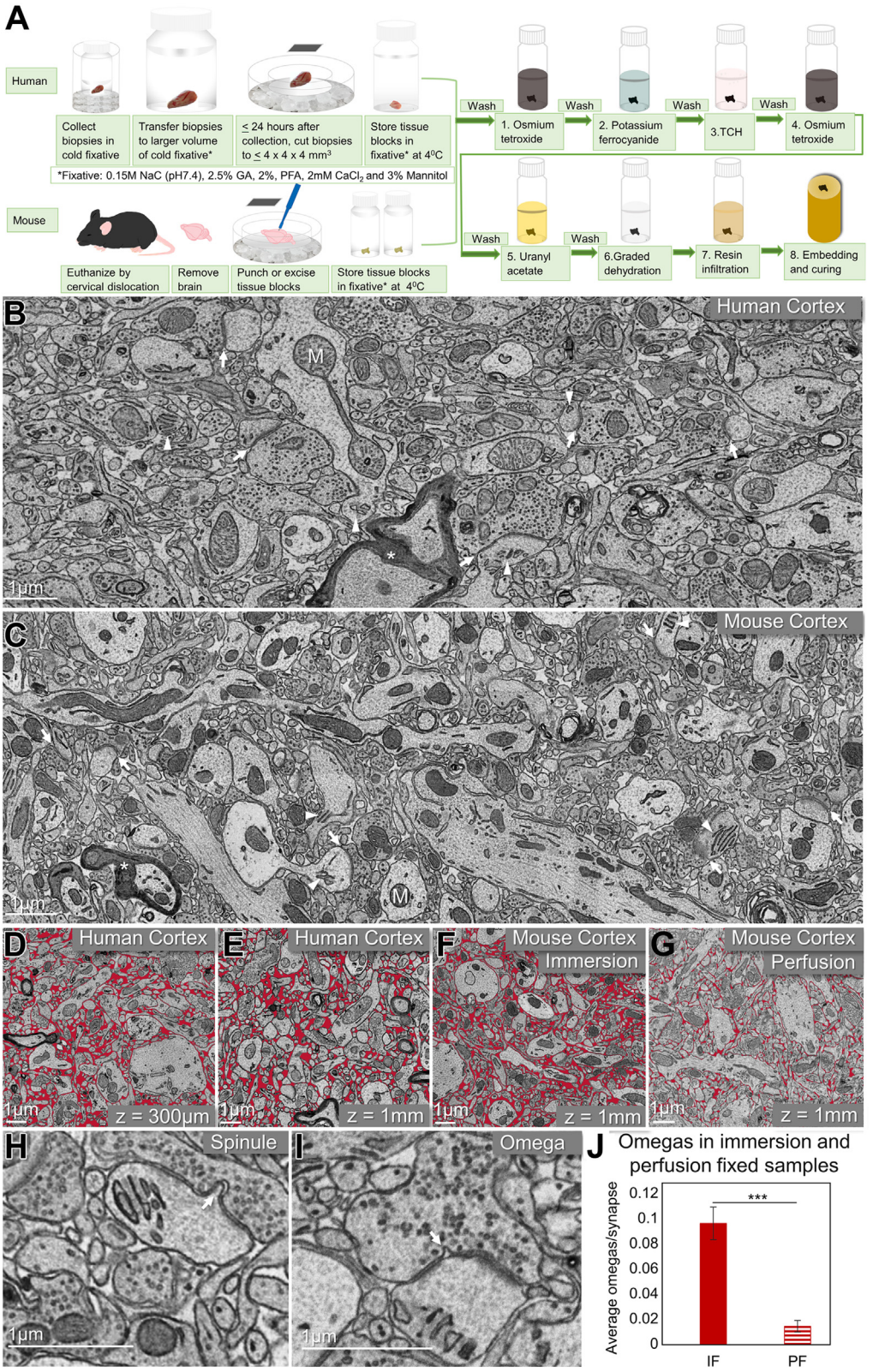

Figure 1. Immersion fixation and heavy metal staining of human and mouse cortical biopsies. **(A)** Shown are the steps for immersion fixation and heavy metal staining of large brain biopsy tissue blocks. **(B)** Electron micrograph from a human brain biopsy ($7.25 \times 3 \times 1.2$ mm^3) taken at a z depth of ~300 µm. The arrows point to synapses, the arrowheads show spine apparatus, M are mitochondria, and the asterisk shows myelin. **(C)** Electron micrograph from mouse

To obtain rodent samples, mice were anesthetized with isoflurane (Baxter) inhalation and euthanized by cervical dislocation. Within 90 seconds of euthanasia, the cerebral cortex was exposed and the brain rostral to the spinal cord was removed and immersed in cold (4 °C) fixative (Table 1 and Figure 1A). To match the clinical retrieval procedure, we used punch biopsies (diameter 1–4 mm) (Ted Pella, Inc.). Four to ten biopsies (along the dorsal-ventral axis) were collected from each mouse brain and were transferred to vials containing cold fixative within 5 minutes from the time of euthanasia (Table 1 and Figure 1A). For transcardiac perfusion fixation, mice were anesthetized with isoflurane, and perfusion was performed as described earlier (9). We used cold fixative (Table 1) for perfusion and then followed the same steps as for the immersion fixation described above.

The method for immersion fixation, heavy metal staining, resin infiltration, and embedding of samples is described in Table 1 (see Key Resources Table for specific reagents used). Screening of samples, sectioning, and image acquisition were done as performed previously (15,28–32) and described in Supplemental Methods (see also Figure 2C, N). Image processing, stitching, alignment, and segmentation of serial section imaged datasets are described in Supplemental Methods (see also Figure 2).

RESULTS

Immersion Fixation

Based on the assessment of many fixation variables (Figure S1), we found that 2.5% glutaraldehyde, 2% paraformaldehyde, and 2mM calcium chloride ($CaCl_2$) in 0.15M sodium cacodylate (NaC) buffered to pH 7.4 provided excellent fixation with immersion in both human and mouse samples. Using 0.15M NaC (295 mOsm) rather than 0.1M NaC (200 mOsm) helped to maintain the ECS, as previously noted (33,34), but was not effective in large-volume samples with a depth of >1 mm. We therefore tested different concentrations of the sugar, mannitol, known to reduce edema and control intracranial volume in patients with traumatic brain injury (35). Mannitol helped preserve ECS when used at 2% ($1 \times 1 \times 1$ mm^3), 3% ($2 \times 2 \times 2$ mm^3), and 3% or 3.5% ($3 \times 3 \times 3$ mm^3) in the fixative solution. However, a higher mannitol concentration (4% w/v) resulted in severe shrinkage of fine cell processes (36,37).

Other ECS maintenance strategies were also tested, including sodium gluconate and the anion channel regulators—DIDS (4,4′-diisothiocyanatostilbene-2,2′-disulfonic acid) and the cystic fibrosis transmembrane conductance regulator antagonist glycine hydrazide (GlyH-101)—as these are thought to reduce neuronal swelling (38). These additional strategies to maintain the ECS were ineffective. Interestingly, DIDS and sodium gluconate noticeably improved contrast at sites of synaptic contact (Figure S2; Key Resources Table).

The temperature of the fixative during immersion and the time from tissue harvesting until immersion had strong effects on the ultimate quality of the ultrastructure. A comparison of fixation of biopsy samples based on temperature was undertaken to assess chilled fixative (4 °C) versus room temperature (RT) fixative. Biopsy samples preserved directly in cold fixatives always had better overall quality when compared with samples immersed in fixative at RT, as previously documented (39). In testing for an acceptable time delay between the tissue harvesting and immersion fixation, we found that an interval of ≥10 minutes between immersion in fixative-free lactated Ringer's solution (270 mOsm) (see Key Resources Table) and the fixative was unacceptable. In particular, ≥10-minute delays caused three ultrastructural abnormalities: broken membranes, mitochondria whose cristae were poorly defined, and large cytoplasm-free vacuoles. Therefore, samples were immersed in cold fixative within 1 minute (human) and within 5 minutes (mouse) after tissue harvesting.

There was little prior information on the duration of immersion fixation for good ultrastructure. To determine the minimal duration of the fixation required, an analysis of immersion fixation was undertaken for blocks $1 \times 1 \times 1$ mm^3 and $2 \times 2 \times 2$ mm^3. At 30 hours for $1 \times 1 \times 1$ mm^3 samples and 46 hours for $2 \times 2 \times 2$ mm^3 samples, the center of the volumes had lower contrast than the periphery, as determined by scanning electron microscopy. In addition to less intensity, the middle of the sample showed poor membrane definition, poor tissue integrity (many small sites where the tissue pulled apart), and poor definition of mitochondrial cristae and difficulty recognizing synapses. Low-staining contrast is often ascribed to poor penetration of osmium tetroxide; however, in this case, the problem was explained by incomplete fixation because the same osmium staining protocol resulted in well-preserved ultrastructure when the fixation step was prolonged to 46 hours ($1 \times 1 \times 1$ mm^3) or 72 hours ($2 \times 2 \times 2$ mm^3). For $3 \times 3 \times 3$ mm^3 and $4 \times 4 \times 4$ mm^3 blocks, fixation for 7 to 28 days resulted in well-preserved ultrastructure. Finally, better membrane preservation of cells and cellular organelles occurred when the fixative contained 2mM $CaCl_2$ versus no $CaCl_2$ (40,41).

Heavy Metal Staining

As described in detail in the flowchart (Figure S1), many staining parameters were altered to achieve uniformly strong osmium and uranium staining without cracks or brittleness in immersion-fixed samples that were at least $2 \times 2 \times 2$ (8) mm^3. The details of each step are provided in Table 1. Eight critical aspects of this protocol are as follows:

cortical block ($2 \times 2 \times 2$ mm^3) taken at a z depth of 1 mm. The arrows, etc., are as in panel **(B)**. **(D)** Electron micrograph from the same human cortical biopsy as shown in panel **(B)**. The ECS is highlighted in red and is 14.5%. **(E)** Electron micrograph from a different human cortical biopsy ($8.25 \times 2.5 \times 1.8$ mm^3) at center of x-y and a z depth of ∼1 mm with 12.2% ECS highlighted in red. **(F)** Electron micrograph of cortex from immersion-fixed mouse biopsy [shown in panel **(C)**] with 13.4% ECS shown in red. **(G)** Electron micrograph from mouse biopsy ($2 \times 2 \times 2$ mm^3) that was obtained after transcardiac perfusion. ECS is diminished (4.9%). **(H)** Electron micrograph from immersion-fixed mouse cortex showing a spinule at a cortical synapse (arrow). **(I)** Electron micrograph from human cortex showing an omega figure at a synapse (arrow). **(J)** Graph showing a significant increase in omega figures in immersion-fixed vs. transcardiac-perfused brain samples (***$p < .0001$, χ^2 test; error bars show SEM). $CaCl_2$, calcium chloride; ECS, extracellular space; GA, glutaraldehyde; IF, immersion fixed; NaC, sodium cacodylate; PF, perfusion fixed; PFA, paraformaldehyde; TCH, thiocarbohydrazide.

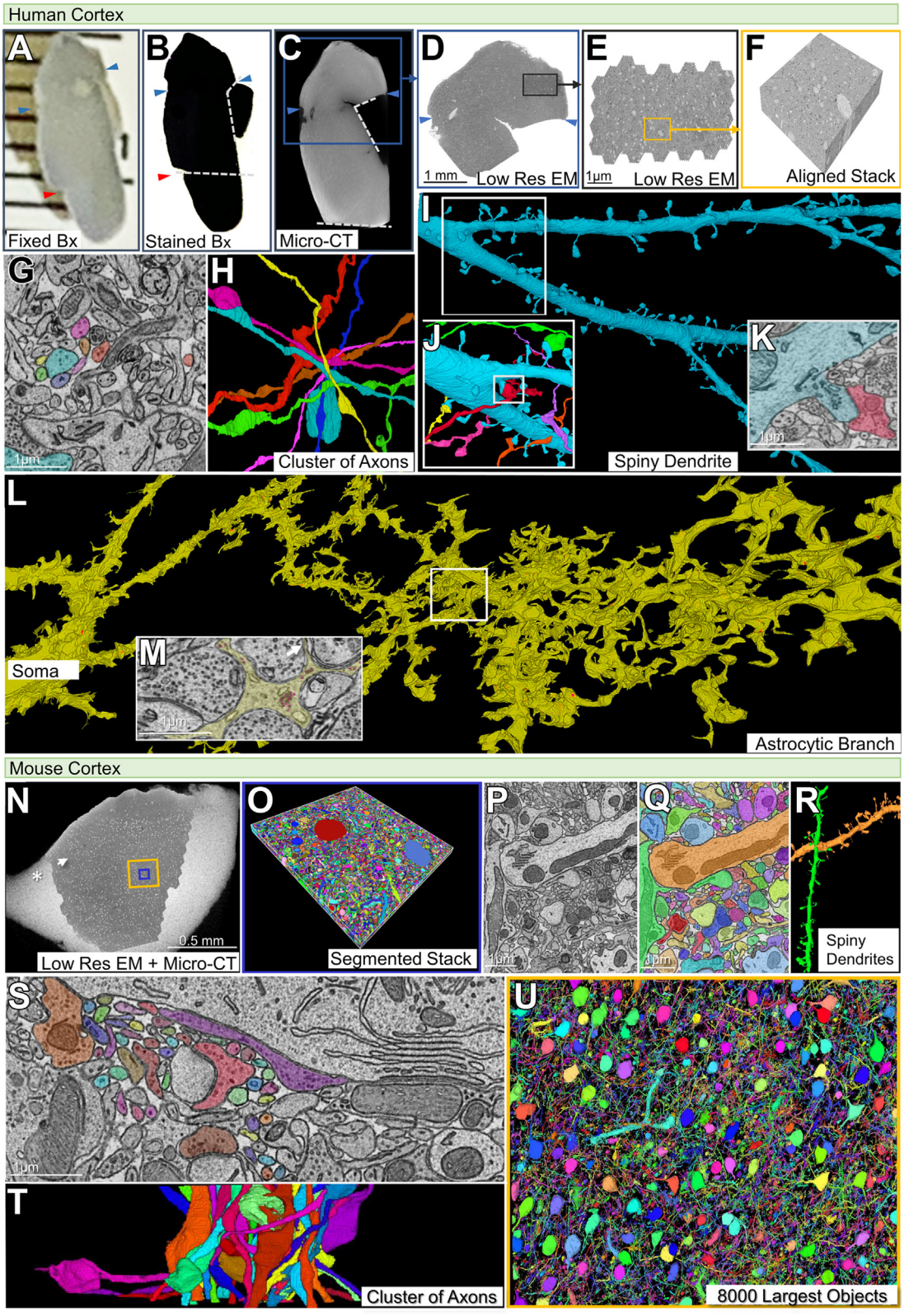
Human Cortex
A
Fixed Bx
B
Stained Bx
C
Micro-CT
D
1 mm
Low Res EM
E
1µm
Low Res EM
F
Aligned Stack
G
1µm
H
Cluster of Axons
I
J
K
1µm
Spiny Dendrite
L
Soma
M
1µm
Astrocytic Branch
Mouse Cortex
N
0.5 mm
Low Res EM + Micro-CT
O
Segmented Stack
P
1µm
Q
1µm
R
Spiny Dendrites
S
1µm
T
Cluster of Axons
U
8000 Largest Objects

1. Multiple NaC buffer washes after aldehyde fixation to lower osmium's opportunity to react with aldehydes, to improve middle-of-the-block staining (42)
2. Osmium tetroxide incubation divided into, first, a 3-hour incubation at RT for fixation of the lipids and, second, a 12-hour incubation at 4 °C for staining
3. An NaC buffer wash prior to potassium ferrocyanide reduction to remove unbound osmium
4. Decreased duration of potassium ferrocyanide to a time less than the first osmium step to mitigate expansion, brittleness of the tissue
5. Addition of 2mM $CaCl_2$ at all steps prior to thiocarbohydrazide (TCH) to increase membrane contrast and lessen breaks
6. Increasing the osmolarity of the vehicle plus reducing the concentration, temperature, and time of TCH reaction to prevent cracks
7. Decreased duration of the second osmium tetroxide staining to a time less than the first osmium step and lowering the incubation temperature to improve contrast
8. Incubation with lower-temperature uranyl acetate to reduce cytoplasmic darkening

Based on these modifications, the tissue fixation and the staining results were excellent in $2 \times 2 \times 2$ (8) mm^3 blocks and in blocks >8 mm^3 when at least one dimension of the block was ≤ 2 mm (Figures 1B–F, 2C, D, N; Figures S3–S5). To investigate the possibility that this protocol might also be useful for blocks in which all three dimensions were >2 mm, incubation times of the various steps were increased, but this approach resulted in cracks and poor staining in the core. For $3 \times 3 \times 3$ (27) mm^3 blocks, more uniform heavy metal staining without cracks was accomplished once (after assessing a range of protocols in 21 blocks) (Figure S1), using a modified protocol (Table S1) that showed sufficient staining at the center point, 1.5 mm from the nearest surface (Figure S6).

To investigate whether this high quality of the ultrastructure could also be obtained with perfusion-fixed, as opposed to immersion-fixed, brain samples, punch biopsies were removed from transcardiac perfusion-fixed mouse brain samples (Methods and Materials), followed by the staining protocol described in Table 1. The ultrastructure was similar in appearance and quality to that obtained with immersion fixation (Figure S7), although the ECS was reduced (Figure 1G). In a $2 \times 2 \times 2$ mm^3 immersion-fixed mouse sample, ECS was on average 15% (20% in layer 1 and 13% in layer 6, SEM $\pm$ 1.3). In the human immersion-fixed samples, ECS was on average 16% (25% at the surface and 12% at the center of the block, SEM $\pm$ 2.8) (Figure 1D–F). In contrast, in a $2 \times 2 \times 2$ (8) mm^3 transcardially perfused sample, the mean ECS was $<5\%$ (range 4.9–4.2, surface to center, SEM $\pm$ 0.35) (Figure 1G; Supplemental Methods).

Ultrastructure in Immersion-Fixed Samples

Use of immersion-fixed samples for connectomic studies requires that synapses, glia, myelin, blood vessels and fine structure is well preserved. The immersion-fixed samples showed well-stained synapses, myelin, mitochondria, blood vessels, and other ultrastructural features that often show abnormalities if poorly fixed or stained (43,44) (Figures 1B, C, 2M and Figure S4) (EM data at https://lichtman.rc.fas.harvard.edu/mouse_cortex_at_1mm). Even in the center of a block that was $8.25 \times 2.5 \times 1.8$ (37) mm^3, the ultrastructure was well preserved (Figure S3). Serial-section stacks of electron micrographs from these blocks revealed several unusual features at sites of close contact between cells, some of which have been reported previously (45–50). For example, small dendritic spinules inserted into axonal boutons (Figure 1H and Figure S8C) and sometimes whole spine heads invaginated into presynaptic axons (Figure S8E, F). Axo-axonal invaginations (Figure S8D), axo-astrocytic and dendro-astrocytic invaginations near synapses (Figure S8G, H), endothelial-endothelial cell invaginations, and pericyte invaginations into the cytoplasm of endothelial cells (Figure S8I, J) were all commonly observed. Red blood cell interactions with endothelial processes in blood vessels were also common. Endothelial microvilli invaginating red blood cells (51) and what seemed to be ejected membrane-bound material from red

Figure 2. Serial section volume collection, imaging, alignment, and segmentation from human and mouse cortical biopsy (Bx.) blocks. **(A)** An immersion-fixed human brain biopsy ($7.25 \times 3 \times 1.2$ mm^3). **(B)** The biopsy shown in panel **(A)** processed with the heavy metal staining ($2 \times 2 \times 2$ mm^3 protocol). The red and blue arrow heads in panels **(A)** and **(B)** show the same regions. Dotted white lines show sites of trimming before resin embedding. **(C)** An x-ray tomogram of the same stained sample, z depth ~300 μm. Dotted white lines are as shown in panel **(B)**. The blue box highlights the region from which a series of 1175 30-nm sections were collected. **(D)** A low-resolution electron micrograph (3×2.5 mm^2) taken from the region highlighted in the blue box in panel **(C)**. Blue arrowheads are the same as in panels **(A)** to **(C)**. The black rectangle shows the region of volume imaged with the multibeam scanning electron microscope. **(E)** Low-resolution 750×250 μm^2 electron micrograph of highlighted rectangle in panel **(D)**. **(F)** An aligned stack of $160 \times 160 \times 35$ μm^3 from the region highlighted with yellow box in panel **(E)**. **(G)** An electron micrograph with cluster of axons traced manually from volume in panel **(F)**. **(H)** Rendering of the manually segmented axons from panel **(G)**; all of them could be traced to two edges of the volume. **(I)** Rendering of a spiny dendrite manually traced from volume in panel **(F)**. **(J)** Inset region from panel **(I)** (changed orientation), showing presynaptic axons making synapses on spines of the blue-colored dendrite in panel **(I)**. **(K)** Electron micrograph of region in white square in panel **(J)** showing a synapse from the red-colored axon onto a dendritic spine. **(L)** Rendering of a manually segmented astrocytic process traced to astrocyte soma. **(M)** A magnified view of an astrocytic process (yellow) and glycogen granules (magenta) from the area within the white box in panel **(L)**. Arrow in panel **(M)** points to a thin process of an astrocyte. **(N)** A low-resolution electron micrograph (shown with arrow) superimposed on an x-ray tomogram (shown with asterisk) at z depth of 1 mm from a $2 \times 2 \times 2$ mm^3 mouse brain biopsy. The yellow box shows 300×300 μm^2 region from which the series of ~100 30-nm sections were aligned and automatically segmented. Automatically segmented region from the blue box is shown in panel **(O)**. **(P)** Electron micrograph with automatic 2D segmentation shown in panel **(Q)**. **(R)** Rendering of two automatically segmented spiny dendrites [green and yellow, as seen in panel **(Q)**]. **(S)** Cluster of automatically segmented axons from yellow boxed area in panel **(N)**. **(T)** Three-dimensional rendering of the axons shown in panel **(S)**. **(U)** A rendering of the 8000 largest objects segmented automatically from the region highlighted with yellow box in panel **(N)**. CT, computed tomography; EM, electron microscopy.

blood cells engulfed by endothelial cells were also observed (Figure S9).

Occasionally, what seemed to be fused vesicles at synapses with an omega shape were observed (Figure 1I) (52–56). These omega figures were seen in both mouse and human brain tissue. Approximately 65% of the synapses in the aligned human cortical sample showed omega figures (64% in excitatory synapses and 70% in inhibitory synapses) (Figure S8A; Supplemental Methods). Similarly, 59% of the synapses in the aligned mouse cortical sample had omega figures (57% in excitatory synapses and 62% in inhibitory synapses) (Figure S8B). Given the rarity of seeing omega figures in previous EM datasets, it is possible that these profiles were related to immersion fixation. Indeed, the incidence of seeing omega profiles was 8-fold greater in immersion-fixed than in perfusion-fixed tissue ($p < .0001$, χ^2 test) (Figure 1J; Supplemental Methods).

Membrane Breaks

Given the deleterious effect of membrane breaks on automatic segmentation, they were assessed for each membrane bound profile in serial-section stacks from samples of immersion-fixed mouse and human blocks that were at least $2 \times 2 \times 2$ (8) mm^3 (Supplemental Methods). There were few breaks: 0.05% in mouse and 0.07% in human samples.

Automated and Manual Segmentation

The ultimate appraisal of ultrastructure quality in connectomics rests on whether neural circuits can be reconstructed. To evaluate this, 1175 images from 30-nm sections were collected at ~300-μm depth from a human sample (Figure 2A–F; Supplemental Methods). Manual reconstruction was straightforward. Eight axons were traced identically by 3 independent annotators. All these axons could be traced to at least two edges of the volume (Figure 2G, H). In addition, two challenging aspects of connectomics data were also traced without difficulty: the spines originating from a spiny dendrite and the many fine terminal processes of an astrocyte (Figure 2I–M). Traced astrocytic processes sometimes narrowed to diameters of <40 nm (Figure 2M); nonetheless, they could be followed until turning into a larger diameter process or leaving the volume. All these results indicate that these large immersion-fixed volumes had excellent staining. Automatic segmentation on a $300 \times 300 \times 3$ μm^3 aligned volume from the center (1-mm depth) of an $2 \times 2 \times 2$ mm^3 mouse brain sample was also tested (Figure 2N–U) (segmentation layer at https://lichtman.rc.fas.harvard.edu/mouse_cortex_at_1mm) (Supplemental Methods). Figure 2U shows the largest 8000 segmented objects, and 77% of these touched the edges of the volume. The negligible membrane breaks observed in this dataset (mentioned above) mitigated most in-plane merge errors. The few merge errors observed were secondary to substrate artifacts as opposed to broken or too faint membrane staining, also indicating the high quality of the immersion fixation and subsequent staining.

DISCUSSION

The goal of this project was to find a method that provided excellent fixation and ultrastructural staining for fresh neurosurgical human biopsies in which perfusion with fixatives was not possible. Because one use of this tissue is connectomics, it was also important that the approach worked well with volumes much larger than 1 mm^3 and had a sufficient amount of ECS to make tracing less difficult. Generating this protocol required modifications to many fixation and heavy metal staining parameters. Each of the staining and washing steps is fraught with some uncertainty about the underlying mechanisms, and optimizing osmium staining is further complicated because this heavy metal has multiple valence states with different reactivities (57). An empirical approach was used to compare the quality of fixation, staining, and tissue penetration using 147 protocol variables in 237 samples and ultimately home in on an optimal protocol (Figure S1).

Several principles of immersion fixation and staining emerged. First, fast transfer (≤5 min) of fresh biopsies to fixative is important. Second, cool temperature (4 °C or RT) is helpful in all steps except resin curing. Third, ECS preservation using mannitol aids fixation, osmium penetration, and segmentation [see also (34)]. Fourth, extensive washing to clear fixatives and unbound osmium resulted in good stain contrast between membranes and cytoplasm. Fifth, a longer first osmium step and a shorter reducing step improved staining and tissue integrity. Sixth, the addition of $CaCl_2$ reduced membrane breaks. In contrast to previous studies, this protocol uses $CaCl_2$ to stabilize membranes from the initial aldehyde fixation step through the potassium ferrocyanide step (4,40,41,45). Seventh, the TCH step was improved by using a lower concentration and in saline as opposed to water. This approach reduced osmotic swelling and gas formation. Eighth, the second osmication needs far less time than the first.

The rapid cold fixation with maintenance of ECS gave ultrastructural features that are less commonly found in traditional cardiac-perfused samples. For example, dendritic spinules and larger invaginations of dendrites into the presynaptic terminal were observed. Such features have been previously described but in smaller blocks and in some samples pristinely prepared via high pressure freezing (45–50,58,59). Additionally, glycogen granules were observed in astrocytic processes as previously described (60–64). However, preservation of these granules is often challenging (62,65), suggesting that the rapid cold immersion approach preserves labile features well. Invaginating processes of blood vessel cells were also observed. Pericytes invaginated endothelial cells, and endothelial cells invaginated each other in ways that were distinct from the classic peg and socket (66) and intercellular tight junctions (67). Finally, many synaptic sites showed synaptic vesicles that were fused with presynaptic terminal membrane (omega figures). Perhaps, these were explained by the rapid cold fixation freezing synaptic release in the act. We cannot, however, discount the possibility that hypertonic mannitol fixative induced vesicle fusion because hypertonic sugar solutions have been used to enhance vesicle fusion events (54,68). One additional advantage of immersion fixation was the more normal ultrastructure of cerebral microvasculature. A caveat of studying microvasculature with EM is that perfusion removes blood cells, limiting analysis of interactions between blood cells and the blood vessel wall. Numerous processes extending between vessel wall and blood cells were observed in these samples. It is hoped that

high-quality preservation of human brain ultrastructure will ultimately provide insight into neurologic and psychiatric questions that have been less accessible with previous approaches.

ACKNOWLEDGMENTS AND DISCLOSURES

This work was funded by the National Institutes of Health (Grant Nos. UG3-MH123386 [to JWL] and U19-NS104653 [to JWL]) and by the National Institute of Mental Health (Grant No. P50MH094271 [to JWL]).

NK and JWL conceived the study. NK designed and performed experiments and collected data. NK and JWL analyzed data. JWL assessed the quality of data. AWC facilitated collection of human cortical biopsies. BHK harvested human cortical biopsies. NK and AWC collected the human biopsies. NK and RLS performed section cutting, screening, and multibeam imaging. YW aligned the human and mouse datasets. NK did manual segmentation in both human and mouse datasets. YM did automatic segmentation of the mouse dataset and computed the largest objects in the volume. NK and YM generated ground truth for automatic segmentation of mouse dataset. DW generated meshes of automatically segmented objects and assessed largest objects. YW wrote the MATLAB script for assessment of extracellular space and for statistical assessment of omegas. NK and JWL wrote the manuscript.

We thank Emily Moya, Lillian Wilkins, You Jeong Park, and Alexander Shapson-Coe for help with human biopsy collections. We thank Olga Morozova for help with animal euthanasia and transcardiac perfusion. We thank Savita Karlupia and Rupali Karlupia for manual segmentation of axons in the human dataset. We thank Sarah Hill for help with counting of fused vesicles and Daniel Berger for technical support with the Volume Annotation and Segmentation Tool.

The results of this study were partially presented at Society for Neuroscience 2021, 2021-S-3404-SfN: Immersion fixation and staining of large volume of human brain tissue for large scale connectomics.

The authors report no biomedical financial interests or potential conflicts of interest.

ARTICLE INFORMATION

From the Department of Molecular and Cellular Biology, Center for Brain Science, Harvard University, Cambridge, Massachusetts (NK, RLS, YW, YM, JWL); Department of Computer Science, Boston College, Boston, Massachusetts (DW); Icahn School of Medicine, Mount Sinai, New York, New York (AWC); and the Center for Neuromodulation, Department of Neurosurgery, The Icahn School of Medicine, Mount Sinai, New York, New York (BHK).

Address correspondence to Neha Karlupia, Ph.D., at nkarlupia@fas.harvard.edu, or Jeff W. Lichtman, M.D., Ph.D., at jeff@mcb.harvard.edu.

Received Aug 6, 2022; revised Jan 25, 2023; accepted Jan 27, 2023.

Supplementary material cited in this article is available online at https://doi.org/10.1016/j.biopsych.2023.01.025.

REFERENCES

1. Hodge RD, Bakken TE, Miller JA, Smith KA, Barkan ER, Graybuck LT, *et al.* (2019): Conserved cell types with divergent features in human versus mouse cortex. Nature 573:61–68.
2. Kasthuri N, Hayworth KJ, Berger DR, Schalek RL, Conchello JA, Knowles-Barley S, *et al.* (2015): Saturated reconstruction of a volume of neocortex. Cell 162:648–661.
3. Morgan JL, Berger DR, Wetzel AW, Lichtman JW (2016): The fuzzy logic of network connectivity in mouse visual thalamus. Cell 165:192–206.
4. Hua Y, Laserstein P, Helmstaedter M (2015): Large-volume en-bloc staining for electron microscopy-based connectomics. Nat Commun 6:7923.
5. Mikula S, Denk W (2015): High-resolution whole-brain staining for electron microscopic circuit reconstruction. Nat Methods 12:541–546.
6. Scheffer LK, Xu CS, Januszewski M, Lu Z, Takemura SY, Hayworth KJ, *et al.* (2020): A connectome and analysis of the adult Drosophila central brain. eLife 9:e57443.
7. Yin W, Brittain D, Borseth J, Scott ME, Williams D, Perkins J, *et al.* (2020): A petascale automated imaging pipeline for mapping neuronal circuits with high-throughput transmission electron microscopy. Nat Commun 11:4949.
8. Witvliet D, Mulcahy B, Mitchell JK, Meirovitch Y, Berger DR, Wu Y, *et al.* (2021): Connectomes across development reveal principles of brain maturation. Nature 596:257–261.
9. Tapia JC, Kasthuri N, Hayworth KJ, Schalek R, Lichtman JW, Smith SJ, Buchanan J (2012): High-contrast en bloc staining of neuronal tissue for field emission scanning electron microscopy. Nat Protoc 7:193–206.
10. MICrONS Consortium, Bae JA, Baptiste M, Bodor AL, Brittain D, Buchanan J, *et al.* (2021): Functional connectomics spanning multiple areas of mouse visual cortex. bioRxiv. https://doi.org/10.1101/2021.07.28.454025.
11. Turner NL, Macrina T, Bae JA, Yang R, Wilson AM, Schneider-Mizell C, *et al.* (2022): Reconstruction of neocortex: Organelles, compartments, cells, circuits, and activity. Cell 185:1082–1100.e24.
12. Morgan JL, Lichtman JW (2013): Why not connectomics? Nat Methods 10:494–500.
13. Lichtman JW, Pfister H, Shavit N (2014): The big data challenges of connectomics. Nat Neurosci 17:1448–1454.
14. Abbott A (2017): Researchers add live human cells to brain database [published online May 30]. Nature. Available at: https://doi.org/10.1038/nature.2017.22889.
15. Shapson-Coe A, Januszewski M, Berger DR, Pope A (2021): A connectomic study of a petascale fragment of human cerebral cortex. bioRxiv. https://doi.org/10.1101/2021.05.29.446289.
16. Loomba S, Straehle J, Gangadharan V, Heike N, Khalifa A, Motta A, *et al.* (2022): Connectomic comparison of mouse and human cortex. Science 377:eabo0924.
17. Cascella N, Butala AA, Mills K, Kim MJ, Salimpour Y, Wojtasievicz T, *et al.* (2021): Deep brain stimulation of the substantia nigra pars reticulata for treatment-resistant schizophrenia: A case report [published correction appears in Biol Psychiatry 2021;90:729]. Biol Psychiatry 90:e57–e59.
18. Singh DR, Bajpai VK, Maitra SC, Shipstone AC, Hasan M (1982): Scanning and transmission electron microscopy of the ependyma of the fourth ventricle in the monkey brain. Acta Anat (Basel) 112:365–375.
19. Eid L, Parent M (2017): Preparation of non-human primate brain tissue for pre-embedding immunohistochemistry and electron microscopy. J Vis Exp 122:55397.
20. Song K, Feng Z, Helmstaedter M (2023): High-contrast en bloc staining of mouse whole-brain and human brain samples for EM-based connectomics. Nat Methods 20:836–840.
21. Beach TG, Tago H, Nagai T, Kimura H, McGeer PL, McGeer EG (1987): Perfusion-fixation of the human brain for immunohistochemistry: Comparison with immersion-fixation. J Neurosci Methods 19:183–192.
22. Castejon OJ (2009): The extracellular space in the edematous human cerebral cortex: An electron microscopic study using cortical biopsies. Ultrastruct Pathol 33:102–111.
23. Witcher MR, Park YD, Lee MR, Sharma S, Harris KM, Kirov SA (2010): Three-dimensional relationships between perisynaptic astroglia and human hippocampal synapses. Glia 58:572–587.
24. Blazquez-Llorca L, Merchán-Pérez Á, Rodríguez JR, Gascón J, DeFelipe J (2013): FIB/SEM technology and Alzheimer's disease: Three-dimensional analysis of human cortical synapses. J Alzheimers Dis 34:995–1013.
25. Domínguez-Álvaro M, Montero-Crespo M, Blazquez-Llorca L, DeFelipe J, Alonso-Nanclares L (2019): 3D electron microscopy study of synaptic organization of the normal human transentorhinal cortex and its possible alterations in Alzheimer's disease. eNeuro 6:ENEURO.0140–19.2019.
26. Yakoubi R, Rollenhagen A, von Lehe M, Miller D, Walkenfort B, Hasenberg M, *et al.* (2019): Ultrastructural heterogeneity of layer 4 excitatory synaptic boutons in the adult human temporal lobe neocortex. eLife 8:e48373.
27. Zhang C, Kim YJ, Silverstein AR, Hoshino A, Reh TA, Dacey DM, Wong RO (2020): Circuit reorganization shapes the developing human foveal midget connectome toward single-cone resolution. Neuron 108:905–918.e3.

28. Hayworth KJ, Morgan JL, Schalek R, Berger DR, Hildebrand DG, Lichtman JW (2014): Imaging ATUM ultrathin section libraries with WaferMapper: A multi-scale approach to EM reconstruction of neural circuits. Front Neural Circuits 8:68.
29. Eberle A, Mikula S, Schalek R, Lichtman JW, Tate MLK, Zeidler D (2015): High-resolution, high-throughput imaging with a multibeam scanning electron microscope. J Microsc 259:114–120.
30. Saalfeld S, Fetter R, Cardona A, Tomancak P (2012): Elastic volume reconstruction from series of ultra-thin microscopy sections. Nat Methods 9:717–720.
31. Meirovitch Y, Matveev A, Saribekyan H, Budden D, Rolnick D, Odor G, *et al.* (2016): A multi-pass approach to large-scale connectomics. arXiv. https://doi.org/10.48550/arXiv.1612.02120.
32. Meirovitch Y, Lu M, Saribekyan H, Matveev A, Rolnick D, Shavit N (2019): Cross-classification clustering: An efficient multi-object tracking technique for 3-D instance segmentation in connectomics. In: Proceedings of the IEEE/CVF Conference on Computer Vision and Pattern Recognition (CVPR). Long Beach: CA, 8425–8435.
33. Karnovsky MJ (1965): A formaldehyde-glutaraldehyde fixative of high osmolality for use in electron microscopy. J Cell Biol 27:1A–149A.
34. Pallotto M, Watkins PV, Fubara B, Singer JH, Briggman KL (2015): Extracellular space preservation aids the connectomic analysis of neural circuits. eLife 4:e08206.
35. Wakai A, McCabe A, Roberts I, Schierhout G (2013): Mannitol for acute traumatic brain injury. Cochrane Database Syst Rev 2013:CD001049.
36. Miyano T, Suzuki A, Sakamoto N (2021): Hyperosmotic stress induces epithelial-mesenchymal transition through rearrangements of focal adhesions in tubular epithelial cells. PLoS One 16:e0261345.
37. Tenny S, Patel R, Thorell W (2022 Jan): Mannitol. In: StatPearls [Internet]. Treasure Island, FL: StatPearls Publishing. Available at: https://www.ncbi.nlm.nih.gov/books/NBK470392/.
38. Rungta RL, Choi HB, Tyson JR, Malik A, Dissing-Olesen L, Lin PJC, *et al.* (2015): The cellular mechanisms of neuronal swelling underlying cytotoxic edema. Cell 161:610–621.
39. Hobro AJ, Smith NI (2017): An evaluation of fixation methods: Spatial and compositional cellular changes observed by Raman imaging. Vib Spectrosc 91:31–45.
40. Forbes MS, Plantholt BA, Sperelakis N (1977): Cytochemical staining procedures selective for sarcotubular systems of muscle: Modifications and applications. J Ultrastruct Res 60:306–327.
41. Hepler PK (1981): The structure of the endoplasmic reticulum revealed by osmium tetroxide-potassium ferricyanide staining. Eur J Cell Biol 26:102–111.
42. Hopwood D (1970): The reactions between formaldehyde, glutaraldehyde and osmium tetroxide, and their fixation effects o bovine serum albumin and on tissue blocks. Histochemie 24:50–64.
43. Hayat MA (1981): Fixation for Electron Microscopy. New York: Academic Press. https://doi.org/10.1016/B978-0-12-333920-1.X5001-0.
44. Glausier JR, Konanur A, Lewis DA (2019): Factors affecting ultrastructural quality in the prefrontal cortex of the postmortem human brain. J Histochem Cytochem 67:185–202.
45. Sorra KE, Fiala JC, Harris KM (1998): Critical assessment of the involvement of perforations, spinules, and spine branching in hippocampal synapse formation. J Comp Neurol 398:225–240.
46. Spacek J, Harris KM (2004): Trans-endocytosis via spinules in adult rat hippocampus. J Neurosci 24:4233–4241.
47. Tao-Cheng JH, Dosemeci A, Gallant PE, Miller S, Galbraith JA, Winters CA, *et al.* (2009): Rapid turnover of spinules at synaptic terminals. Neuroscience 160:42–50.
48. Petralia RS, Wang YX, Mattson MP, Yao PJ (2018): Invaginating structures in mammalian synapses. Front Synaptic Neurosci 10:4.
49. Petralia RS, Yao PJ, Kapogiannis D, Wang YX (2021): Invaginating structures in synapses - Perspective. Front Synaptic Neurosci 13: 685052.
50. Wood BM, Baena V, Huang H, Jorgens DM, Terasaki M, Kornberg TB (2021): Cytonemes with complex geometries and composition extend into invaginations of target cells. J Cell Biol 220:e202101116.
51. Makarov V, Zueva L, Sanabria P, Wessinger WD, Golubeva T, Khmelinskii I, Inyushin M (2015): On the role of the blood vessel endothelial microvilli in the blood flow in small capillaries. J Biophys 2015:529746.
52. Heuser JE, Reese TS, Landis DM (1974): Functional changes in frog neuromuscular junctions studied with freeze-fracture. J Neurocytol 3:109–131.
53. Heuser JE, Reese TS, Dennis MJ, Jan Y, Jan L, Evans L (1979): Synaptic vesicle exocytosis captured by quick freezing and correlated with quantal transmitter release. J Cell Biol 81:275–300.
54. Heuser JE, Reese TS (1981): Structural changes after transmitter release at the frog neuromuscular junction. J Cell Biol 88:564–580.
55. Heuser JE (1989): Review of electron microscopic evidence favouring vesicle exocytosis as the structural basis for quantal release during synaptic transmission. Q J Exp Physiol 74:1051–1069.
56. Jung JH, Szule JA, Stouder K, Marshall RM, McMahan UJ (2018): Active zone material-directed orientation, docking, and fusion of dense core vesicles alongside synaptic vesicles at neuromuscular junctions. Front Neuroanat 12:72.
57. White DL, Andrews SB, Faller JW, Barrnett RJ (1976): The chemical nature of osmium tetroxide fixation and staining of membranes by x-ray photoelectron spectroscopy. Biochim Biophys Acta 436:577–592.
58. Rodriguez-Moreno J, Rollenhagen A, Arlandis J, Santuy A, Merchan-Pérez A, DeFelipe J, *et al.* (2018): Quantitative 3D ultrastructure of thalamocortical synapses from the "lemniscal" ventral posteromedial nucleus in mouse barrel cortex. Cereb Cortex 28:3159–3175.
59. Rollenhagen A, Walkenfort B, Yakoubi R, Klauke SA, Schmuhl-Giesen SF, Heinen-Weiler J, *et al.* (2020): Synaptic organization of the human temporal lobe neocortex as revealed by high-resolution transmission, focused ion beam scanning, and electron microscopic tomography. Int J Mol Sci 21:5558.
60. De Bruijn WC, Den Beejen P (1975): Glycogen, its chemistry and morphological appearance in the electron microscope.11. The complex formed in the selective contrast staining of glycogen. Histochem J 7:205–229.
61. de Bruijn WC, Den Breejen P (1976): Glycogen, its chemistry and morphological appearance in the electron microscope. III. Identification of the tissue ligands involved in the glycogen contrast staining reaction with the osmium (VI)–iron(II) complex. Histochem J 8:121–142.
62. Fiala JC, Kirov SA, Feinberg MD, Petrak LJ, George P, Goddard CA, Harris KM (2003): Timing of neuronal and glial ultrastructure disruption during brain slice preparation and recovery in vitro. J Comp Neurol 465:90–103.
63. Bamisi OD, Alese MO (2020): Effects of various fixatives and temperature on the quality of glycogen demonstration in the brain and liver tissues. Ann Diagn Pathol 48:151604.
64. Zakout YMA, Salih MM, Ahmed HG (2010): The effect of fixatives and temperature on the quality of glycogen demonstration [published correction appears in Biotech Histochem 2011;86:448]. Biotech Histochem 85:93–98.
65. Woods AE, Stirling JW (2019): Transmission electron microscopy. In: Suvarna SK, Layton C, Bancroft JD, editors. Bancroft's Theory and Practice of Histological Techniques. Amsterdam: Elsevier, 434–475.
66. Ornelas S, Berthiaume AA, Bonney SK, Coelho-Santos V, Underly RG, Kremer A, *et al.* (2021): Three-dimensional ultrastructure of the brain pericyte-endothelial interface. J Cereb Blood Flow Metab 41:2185–2200.
67. Dejana E, Orsenigo F, Molendini C, Baluk P, McDonald DM (2009): Organization and signaling of endothelial cell-to-cell junctions in various regions of the blood and lymphatic vascular trees. Cell Tissue Res 335:17–25.
68. Rosenmund C, Stevens CF (1996): Definition of the readily releasable pool of vesicles at hippocampal synapses. Neuron 16:1197–1207.